TIME-VARYING STAP FOR NONSTATIONARY HOT CLUTTER CANCELLATION

Giuseppe A. Fabrizio

National Security and ISR Division,
DSTO Edinburgh, Australia.

Alfonso Farina

Selex ES,
Via Tiburtina, km 12.4, 00131, Rome, Italy.

ABSTRACT

This paper addresses the problem of mitigating non-stationary diffusely scattered multipath interference or "hot clutter" by space-time adaptive processing (STAP) in radar systems that use a multi-channel receive antenna array. A computationally efficient time-varying (TV) fast-time STAP algorithm that can effectively cancel hot clutter during the coherent processing interval (CPI) while simultaneously preserving the Doppler spectrum characteristics of the ordinary backscattered "cold clutter" is proposed. The TV-STAP method is compared with several benchmark techniques in a numerical study simulating aircraft and ship detection in over-the-horizon (OTH) radar.

***Index Terms*—** STAP, OTH Radar, Hot Clutter

1. INTRODUCTION

The topic of space-time adaptive processing (STAP) to mitigate clutter and interference in radar systems has received enormous attention in the literature [1-3]. In particular, the "fast-time" STAP architecture is traditionally considered for the specific problem of rejecting diffuse multipath interference, or "hot clutter", which may be received through the main lobe of the antenna pattern [4-6].

In practical applications, the space-time covariance matrix of the received hot-clutter signal may be time-varying over the radar CPI. For this reason, STAP techniques that can jointly cancel the non-stationary hot clutter signal and preserve the Doppler spectrum characteristics of the backscattered "cold clutter" echoes over the CPI are required [7].

The stochastic constraints (SC) STAP method pioneered by Abramovich has been described in [8-10] to address this challenging problem. The SC-STAP method adapts the weight vector at every pulse in the CPI to effectively reject hot clutter while stabilizing the auto-regressive spectral characteristics of cold clutter at the output.

However, SC-STAP is computationally intensive for real-time applications. This is mainly because the rate of filter adaptation is determined by the need to protect the AR Doppler spectrum properties of the cold clutter, irrespective of the level of hot-clutter non-stationarity, which ought to be the primary reason for re-adapting the STAP weights [11].

For practical systems, this strongly motivates fast-time TV-STAP algorithms that are computationally efficient while, at the same time, yield high performance comparable to the SC-STAP method. The TV-STAP method introduced in this paper follows the same basic idea as the SC-STAP technique, but is structured differently to mitigate the aforementioned limitation of the original approach proposed for OTH radar.

The paper is organized as follows. Section 2 describes the data model, while section 3 presents the TV-STAP method. The numerical study in section 4 compares the performance of SC-STAP, TV-STAP, and the time-invariant fast-time STAP technique. Concluding remarks are given in section 5.

2. DATA MODEL

Let $\mathbf{x}_k(t) \in \mathcal{C}^N$ be the array snapshot vector received by the N antenna elements of a uniform linear array (ULA) at fast-time sample (range bin) $k = 1, \dots, K$ and slow-time sample (pulse number) $t = 1, \dots, P$ in the radar CPI. In (1), $\mathbf{c}_k(t)$ is the cold clutter backscattered from the Earth's surface, $\mathbf{j}_k(t)$ is hot clutter from all jamming sources, and $\mathbf{n}_k(t)$ is additive noise. The presence of a target echo is represented by $\mathbf{s}_k(t)$.

$$\mathbf{x}_k(t) = \mathbf{s}_k(t) + \mathbf{c}_k(t) + \mathbf{j}_k(t) + \mathbf{n}_k(t) \tag{1}$$

A far-field point-target echo with cone angle-of-arrival φ_0 is modelled in (2), where a is a complex scalar amplitude, ψ_k is the signal waveform, f_d is the target Doppler-shift normalized by the pulse repetition frequency (PRF), $\mathbf{s}(\varphi_0)$ is the steering vector on the ULA manifold, and γ_k is a range-dependent phase. A desired signal matched to range bin k_0 has a fast-time signature $\psi_k = \delta(k - k_0)$ for a pulsed-waveform system. For a continuous-wave system, $\psi_k = u_p(k - k_0)$, where $u_p(k)$ is the transmitted signal pulse.

$$\mathbf{s}_k(t) = a\psi_k \mathbf{s}(\varphi_0) \exp\{j2\pi f_d t + \gamma_k\} \tag{2}$$

The noise process is assumed to be complex-circular Gaussian distributed and white across all radar data-cube dimensions, i.e., with the correlation properties in (3), where σ_n^2 is the noise power per antenna element, and $\mathbf{I}_N$ is the N-dimensional identity matrix. In (3), $\mathrm{E}\{\cdot\}$ denotes statistical expectation, whereas $\dagger$ is the Hermitian (conjugate transpose) operator.

$$\mathrm{E}\{\mathbf{n}_k(t)\mathbf{n}_{k'}^{\dagger}(t')\} = \delta_{kk'}\delta tt'\mathbf{I}_N \tag{3}$$

2.1. Cold Clutter

As in [9], $\mathbf{c}_k(t)$ is modelled as a stationary Gaussian random process with second order statistics given by a *scalar-type* multi-variate auto-regressive (AR) process of relatively low order $\kappa \ll N$. The complex scalar coefficients $\{b_i\}_{i=1}^{\kappa}$ and σ_ε^2 of the AR model in (4) determine the structure and scale of the cold clutter Doppler power spectrum, respectively.

$$\mathbf{c}_k(t) + \sum_{i=1}^{\kappa} b_i \mathbf{c}_k(t-i) = \sigma_\varepsilon^2 \underline{\varepsilon}_k(t) \qquad (4)$$

The correlation properties of the temporally white innovative noise vectors $\underline{\varepsilon}_k(t) \in \mathcal{C}^N$ in (5) effect the power and spatial distribution of the cold clutter. Due to the relatively broad transmit beam used to illuminate the OTH radar surveillance region, the cold clutter is spatially broadband such that $\mathbf{R}_c$ has full rank. For a spatially stationary clutter process, $\mathbf{R}_c$ is a Toeplitz matrix with diagonal elements equal to the clutter power σ_c^2 received in each antenna element.

$$\mathrm{E}\left\{\underline{\varepsilon}_k(t)\underline{\varepsilon}_{k'}^{\dagger}(t')\right\} = \delta_{kk'}\delta_{tt'}\mathbf{R}_c \qquad (5)$$

A simple model for the spatial distribution of the cold clutter assumes $\mathbf{R}_c = \sigma_c^2 \mathrm{Toep}[1, \rho_s, \ldots, \rho_s^{N-1}]$, where the complex scalar ρ_s represents the clutter inter-sensor spatial correlation coefficient. Similarly, AR model orders of $\kappa = 1$ and $\kappa = 2$ may be assumed in the simplest case for high and low PRF operation, respectively.

2.2. Hot Clutter

The hot clutter $\mathbf{j}_k(t)$ is modelled as a convolutive mixture of M interference sources $g_{mk}(t)$ for $m = 1, \ldots, M$ in (6). Here, $\mathbf{g}_k(t) = [g_{1k}(t), \ldots, g_{Mk}(t)]^T$ contains the M source signals. The $N \times M$ matrix $\mathbf{H}_\ell(t) = [\mathbf{h}_{1\ell}(t), \ldots, \mathbf{h}_{M\ell}(t)]$ contains the hot-clutter wavefronts $\mathbf{h}_{m\ell}(t)$ at fast-time k and slow-time t. Note that L is the maximum hot clutter channel impulse response function duration in fast-time samples [9].

$$\mathbf{j}_k(t) = \sum_{\ell=1}^{L} \mathbf{H}_\ell(t)\mathbf{g}_{k-\ell+1}(t) \qquad (6)$$

Specifically, the $(n, m)^{\text{th}}$ element of $\mathbf{H}_\ell(t)$ is the complex channel coefficient that transfers source m to receiver n at relative delay ℓ in repetition period t. The waveforms $g_{mk}(t)$ are assumed to be mutually independent with the correlation properties in (7). Note that the power of each hot-clutter mode is absorbed in the channel vectors $\mathbf{h}_{m\ell}(t)$ described below.

$$\mathrm{E}\left\{g_{mk}(t)g_{m'k'}^{*}(t')\right\} = \delta_{mm'}\delta_{tt'}\delta_{kk'} \qquad (7)$$

The random vectors $\mathbf{h}_{m\ell}(t)$ are assumed to be independent for different sources and modes. In (8), $A_{m\ell}$ and $f_{m\ell}$ denote the RMS amplitude and Doppler shift of mode ℓ from source m, respectively, while the $N \times N$ matrix $\mathbf{S}_{m\ell}$ represents the mean synthetic wavefront of this mode in the CPI. The vector $\mathbf{c}_{m\ell}(t)$ incorporates the random spatio-temporal fluctuations of the received hot clutter wavefronts. This accounts for the DOA and Doppler spread imposed on the various sources and modes. See [7,12] for a detailed description of this model.

$$\mathbf{h}_{m\ell}(t) = A_{m\ell}\mathbf{S}_{m\ell}\mathbf{c}_{m\ell}(t)\exp\{j2\pi f_{m\ell}t\} \qquad (8)$$

The simplest model for $\mathbf{c}_{m\ell}(t)$ is a two-dimensional (space-time) Markov chain defined by two parameters, namely, a temporal correlation coefficient $\alpha_{m\ell}$, and a spatial correlation coefficient $\beta_{m\ell}$. Lower values of $\alpha_{m\ell}$ and $\beta_{m\ell}$ correspond to modes with rapid temporal fluctuations and large wavefront "crinkles". For $q = 0, \ldots, Q-1$, the fast-time-lagged hot clutter covariance matrix $\mathbf{R}_q(t) = E\{\mathbf{j}_k(t)\mathbf{j}_{k-q}^{\dagger}(t)\}$ is given by (9). Clearly, $\mathbf{R}_q(t) = \mathbf{0}$ for $q \geq L$ since there is no pair of modes with a differential delay exceeding the maximum impulse response duration of the hot clutter channel.

$$\mathbf{R}_q(t) = \sum_{m=1}^{M}\sum_{\ell=1}^{L-q} A_{m\ell}A_{m\ell+q}\mathbf{S}_{m\ell}\mathbf{c}_{m\ell}(t)\mathbf{c}_{m\ell+q}^{\dagger}(t)\mathbf{S}_{m\ell+q}^{\dagger} \qquad (9)$$

The hot-clutter space-time covariance matrix for Q fast-time taps in (10) remains constant during the "quasi-instantaneous" PRI but changes in slow-time t over the relatively long CPI to represent the non-stationarity hot clutter phenomenon.

$$\tilde{\mathbf{R}}(t) = \mathrm{Toep}[\mathbf{R}_0(t), \mathbf{R}_1(t), \ldots, \mathbf{R}_{Q-1}(t)] \qquad (10)$$

3. STAP ALGORITHM

Fast-time STAP algorithms operate on NQ-variate "stacked" data vectors $\tilde{\mathbf{x}}_k(t)$ defined in (11), and the scalar output $z_k(t)$ processed by the NQ-variate STAP filter $\tilde{\mathbf{w}}_k(t)$ is given by $z_k(t) = \tilde{\mathbf{w}}_k^{\dagger}(t)\tilde{\mathbf{x}}_k(t)$. Note that this filter does *not* attempt to cancel the cold clutter, which is dealt with by standard Doppler processing of the "finger beam" output $z_k(t)$.

$$\tilde{\mathbf{x}}_k(t) = \left[\mathbf{x}_k(t)^T, \mathbf{x}_{k-1}(t)^T, \ldots, \mathbf{x}_{k-Q+1}(t)^T\right]^T \qquad (11)$$

The practical TV-STAP procedure replaces the unknown matrix $\tilde{\mathbf{R}}(t)$ by its regularized sample estimate $\hat{\mathbf{R}}_b$ in (12). Averaging is performed over N_k fast-time samples containing hot-clutter only in N_p consecutive pulses belonging to integer batch number $b = 1, \ldots, N_b = P/N_p$ of the CPI.

$$\hat{\mathbf{R}}_b = \frac{1}{N_p N_k}\sum_{t=(b-1)N_p+1}^{bN_p+\kappa}\sum_{k=1}^{N_k}\tilde{\mathbf{x}}_k(t)\tilde{\mathbf{x}}_k^{\dagger}(t) + \sigma^2\mathbf{I}_{NQ} \qquad (12)$$

The practical TV-STAP algorithm is formulated in terms of q deterministic and κ data-driven linear constraints in (13). The former are defined by $\mathbf{A}_Q(\theta) = \mathbf{s}(\varphi_0) \otimes \mathbf{I}_Q$, where $\otimes$ is the Kronecker product, and $\mathbf{e}_Q = [1, 0, \ldots, 0]^T$. The latter take the form of $\mathbf{w}^\dagger \tilde{\mathbf{x}}_k(t) = \hat{\mathbf{w}}_k^\dagger(b-1)\tilde{\mathbf{x}}_k(t)$ for slow-time samples $t = N_p(b-1), \ldots, N_p(b-1)+\kappa-1$ in batch b.

$$\hat{\mathbf{w}}_k(b) = \arg\min_{\mathbf{w}} \ \mathbf{w}^\dagger \hat{\mathbf{R}}_b \mathbf{w} \quad \text{subject to} \begin{cases} \mathbf{w}^\dagger \mathbf{A}_Q(\theta) = \mathbf{e}_Q^T, \\ \mathbf{w}^\dagger \tilde{\mathbf{x}}_k(t) = \hat{\mathbf{w}}_k^\dagger(b-1)\tilde{\mathbf{x}}_k(t) \end{cases} \tag{13}$$

The first STAP filter ($b = 1$) has only deterministic constraints and is $\hat{\mathbf{w}}_k(1) = \hat{\mathbf{R}}_1^{-1}\mathbf{A}_Q(\theta)[\mathbf{A}_Q(\theta)^\dagger \hat{\mathbf{R}}_1^{-1}\mathbf{A}_Q(\theta)]^{-1}\mathbf{e}_Q$. For batches $b = 2, \ldots, N_b$, the STAP filter also satisfies the data-driven constraints and is given by (14).

$$\hat{\mathbf{w}}_k(b) = \hat{\mathbf{R}}_b^{-1}\hat{\mathbf{C}}_k(b)[\hat{\mathbf{C}}_k^\dagger(b)\hat{\mathbf{R}}_b^{-1}\hat{\mathbf{C}}_k(b)]^{-1}\hat{\mathbf{f}}_k(b) \tag{14}$$

Here, $\hat{\mathbf{C}}_k(b) = [\mathbf{A}_q(\theta_0), \tilde{\mathbf{x}}_k(N_p(b-1)), \ldots, \tilde{\mathbf{x}}_k(N_p(b-1)+\kappa-1)]$ is the constraint matrix and $\hat{\mathbf{f}}_k(b) = [\mathbf{e}_q^T, \hat{\mathbf{w}}_k^\dagger(b-1)\tilde{\mathbf{x}}_k(N_p(b-1)), \ldots, \hat{\mathbf{w}}_k^\dagger(b-1)\tilde{\mathbf{x}}_k(N_p(b-1)+\kappa-1))]^T$ is the response vector. In the interest of brevity, the reader is referred to [9] for a description of the SC-STAP method, which serves as benchmark for comparisons in the next section.

TV-STAP reduces the number of complex multiplications relative to SC-STAP by a factor that is closely approximated by the batch length N_p. For example, if the hot clutter can be considered effectively "stationary" over a ship-detection pulse with 4 Hz PRF, the same signal may also be considered stationary over 15 consecutive air-detection pulses at a PRF of 60 Hz, as the physical time interval is unchanged. In this case, TV-STAP using $N_p = 16$ may be expected to cancel the hot clutter as effectively as SC-STAP with an order of magnitude reduction in computational load.

4. SIMULATION RESULTS

Assume the radar transmits $P = 256$ pulses and receives on a ULA of $N = 16$ antennas with half-wavelength inter-element spacing. The beam is steered at broadside and there is single hot clutter source with four modes ($M = 1$, $L = 4$). The hot clutter model parameters are listed in Table 1. The DOA of the first mode is intentionally chosen in the main beam to demonstrate the benefit of fast-time STAP over pure SAP. The temporal hot clutter parameters have been specified for low and high PRF modes. HCNR denotes hot-clutter-to-noise ratio. The model parameters of the cold clutter are listed in Table 2 for terrain ($\kappa = 1$) and sea surface ($\kappa = 2$) scattering.

Hot Clutter	$\theta_{m\ell}$, deg.	$\alpha_{m\ell}$(5 Hz)	$\alpha_{m\ell}$(50 Hz)	$\beta_{m\ell}$	HCNR, dB
Mode 1	0.5	1.00	1.00	1.00	30
Mode 2	20.5	0.90	0.98	0.91	25
Mode 3	39.3	0.88	0.97	0.90	20
Mode 4	44.9	0.91	0.99	0.90	35

Table 1. Hot clutter parameters for a source with four modes.

Fig. 1 shows the optimum SHCR for different schemes in the "clairvoyant" case. The term unconstrained refers to no data-driven constraints. As expected, unconstrained STAP

Cold Clutter	b_1	b_2	σ_ε^2	ρ_s	CNR, dB
Sea-surface, $f_p = 5$ Hz	-1.9359	0.998	0.009675	0.5	50
Terrain, $f_p = 50$ Hz	0.999	0	0.002	0.5	50

Table 2. Cold clutter parameters for terrain and sea scattering.

rejects the hot clutter best ($Q = 3$ taps were used for all STAP schemes). Unconstrained SAP is ineffective due to the presence of main beam hot clutter, while time-invariant STAP cannot cancel the non-stationary hot clutter effectively.

Fig. 2 illustrates the cold-clutter Doppler spectrum at the output of the unconstrained and time-invariant STAP filters as well SC-STAP filter using the second-order AR (sea-scattering) model. The dramatic degradation in sub-clutter visibility (SCV) is obvious when unconstrained STAP is applied. Fig. 3 confirms that the cold-clutter Doppler spectra at the output of SC-STAP and TV-STAP have practically identical SCV to the time-invariant STAP approach.

Figs. 4 and 5 show the performance of the practical STAP schemes, where the hot-clutter covariance matrix is estimated from training data, and data snapshots containing hot and cold clutter are used to generate the auxiliary data-driven linear constraints. A total of $N_k = 50$ training range cells in each PRI were deemed to be free of cold clutter. These results confirm that TV-STAP can reduce computational complexity for negligible performance loss in the ship-detection case.

Figs. 6 and 7 show the Doppler spectra for practical STAP schemes in the high PRF example. In this case, both SC-STAP and TV-STAP employ a single auxiliary linear constraint to protect SCV. Fig. 7 compares SC-STAP with TV-STAP using a batch length of $N_p = 16$ pulses. This batch length provides an order of magnitude reduction in computational load with respect to SC-STAP for negligible loss in hot-clutter rejection. Both SC-STAP and TV-STAP detect the desired signal in Fig. 7, but time-invariant STAP leads to a degradation in hot clutter rejection of about 25 dB in Fig. 6.

5. CONCLUSIONS

A TV-STAP technique has been introduced for non-stationary hot clutter cancellation. Simulation results confirm that TV-STAP can yield comparable performance to the benchmark SC-STAP method. However, the philosophy behind TV-STAP is to update the filter weights at a rate commensurate with the level of hot clutter non-stationarity rather than at every PRI to stabilize the AR characteristics of the output cold-clutter Doppler spectrum. This difference with respect to SC-STAP gives TV-STAP the added practical advantage of significantly reduced computational complexity. The order of magnitude reduction in processing load achieved by TV-STAP in high PRF applications helps to break the bottleneck of real-time processing in practical radar systems with no compromise in performance on the simulated data presented in this study. See [13] for a possible real-time implementation procedure. Testing on experimental data is the subject of future work.

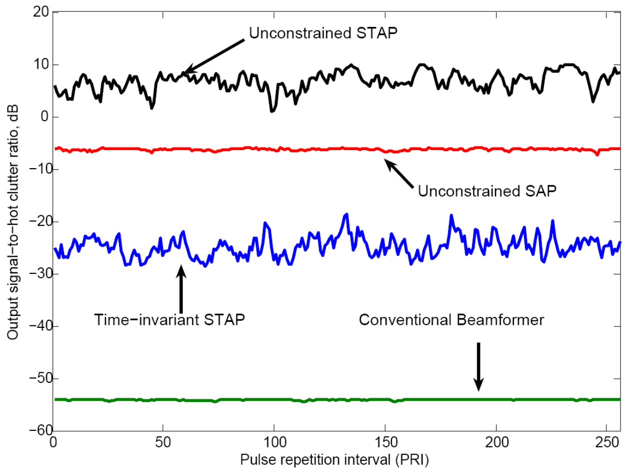

Fig. 1. Optimum output signal-to-hot clutter ratio (SHCR) for standard fast-time STAP and pure spatial adaptive processing (SAP) as a function of slow-time over the CPI.

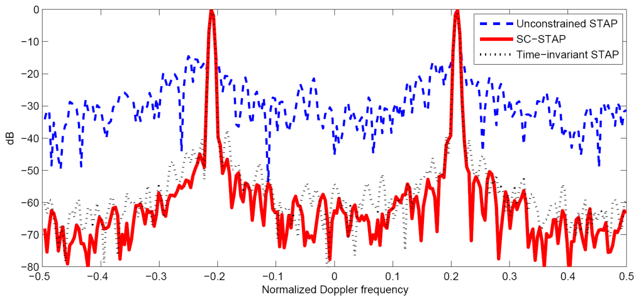

Fig. 2. Doppler spectra showing the sub-clutter visibility at the output of the standard STAP techniques and the SC-STAP method when processing the cold clutter.

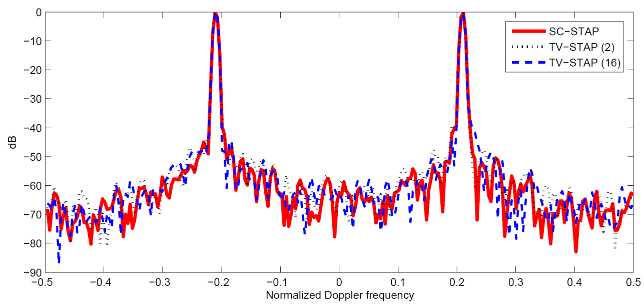

Fig. 3. Doppler spectra showing the sub-clutter visibility at the output of SC-STAP and TV-STAP using different batch lengths when processing the cold clutter.

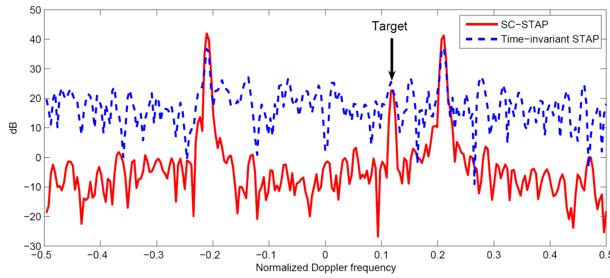

Fig. 4. Doppler spectra for the practical time-invariant STAP and SC-STAP algorithms in the ship detection example with an injected desired signal.

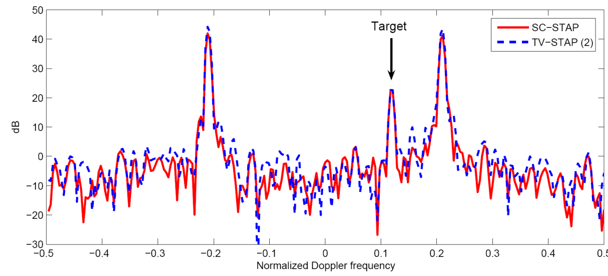

Fig. 5. Doppler spectra for practical SC-STAP and TV-STAP in the ship detection example with an injected desired signal.

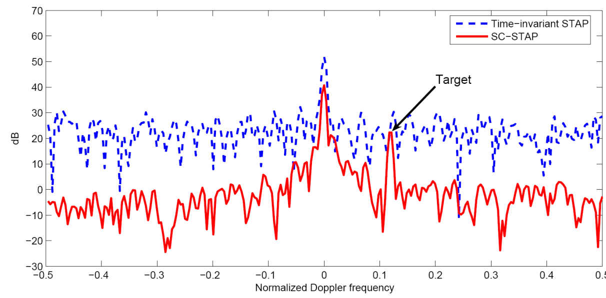

Fig. 6. High PRF mode Doppler spectra for practical time-invariant STAP and SC-STAP algorithms in the aircraft detection example with an injected target.

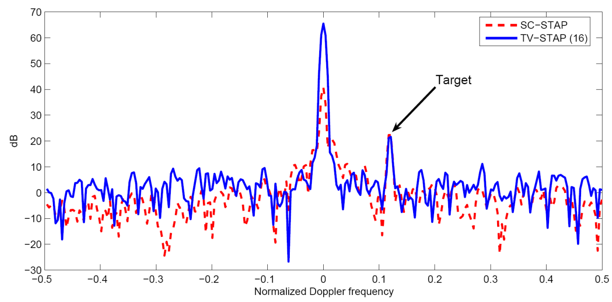

Fig. 7. High PRF Doppler spectra for practical SC-STAP and TV-STAP algorithms in the aircraft detection example with an injected target.

6. REFERENCES

[1] Klemm, R.: Applications of Space-Time Adaptive Proceesing, The Institution of Electrical Engineers, London, UK, 2004.

[2] Guerci, J. R.: Space-Time Adaptive Processing for Airborne Radar, Artech House, Norwood, MA, 2003.

[3] Melvin, W.: A STAP overview, IEEE Aerospace and Electronic Sytems Magazine 19(1), 2004, 19-35.

[4] Fante, R. and Torres, J. A.: Cancellation of diffuse jammer multipath by an airborne adaptive radar, IEEE Transactions on Aerospace and Electronic Systems 31(2), 1995, 805-820.

[5] Jouny, I. I. and Culpepper, E.: Modeling and mitigation of terrain scattered interference, Proceedings of IEEE International Symposium on Antennas and Propagation 1, 1995, 455-457.

[6] Kogon, S. M., Williams, D. B., and Holder, E. J.: Exploiting coherent multipath for main beam jammer suppression, IEE Proceedings - Radar, Sonar and Navigation 145(5), 1998, 303-308.

[7] Fabrizio, G. A.: High Frequency Over-the-Horizon Radar: Fundamental Principles, Signal Processing, and Practical Applications, McGraw-Hill, NY, 2013, 659–664.

[8] Anderson, S. J., Abramovich, Y. I., and Fabrizio, G. A.: Stochastic constraints in nonstationary hot clutter cancellation, IEEE International Conference on Acoustics, Speech and Signal Processing (ICASSP-97), Munich, Germany, 1997, 3753-3756.

[9] Abramovich, Y. I., Spencer, N. K., Anderson, S. J., and Gorokhov, A. Y.: Stochastic constraints method in nonstationary hot-clutter cancellation, Part 1: Fundamentals and supervised training applications, IEEE Transactions on Aerospace and Electronic Systems 34(4), 1998, 1271-1292.

[10] Abramovich, Y. I., Anderson, S. J., and Spencer, N.: Stochastic-constraints method in nonstationary hot-clutter cancellation, Part 2: Unsupervised training applications, IEEE Transactions on Aerospace and Electronic Systems 36(1), 2000, 132-150.

[11] Fabrizio, G. A., Gershman, A. B., and Turley, M. D.: Robust adaptive beamforming for HF surface wave over-the-horizon radar, IEEE Transactions on Aerospace and Electronic Systems 40(2), 2004, 510-525.

[12] Abramovich, Y. I., Gorokhov, A. Y., and Demeure, C.: Experimental verification of a generalized multivariate propagation model for ionospheric HF signals, Proceedings of the European Signal Processing Conference (EUSIPCO-96), Trieste, Italy, 1996, 1853-1856.

[13] Farina, A., Saverione, A., Timmoneri, L.: The MVDR vectorial lattice applied to space-time processing for AEW radar with large instantaneous bandwidth, IEE Proc. Radar, Sonar and Navigation, 143(1), 1996, 41–46.